ACS EARTH AND SPACE CHEMISTRY

http://pubs.acs.org/journal/aesccq

Article

NOM-Induced Dissolution of $Cr_xFe_{1-x}(OH)_3$ Precipitates and Formation of Cr(III)-NOM-Fe Colloids under Oxic and Anoxic Conditions

Binrui Li,[‖] Shaojian Zhang,[‖] Peng Liao,* Peng Liu, Zhihang Ye, and Chongxuan Liu*

Cite This: *ACS Earth Space Chem.* 2022, 6, 2995−3006

Read Online

ACCESS | Metrics & More | Article Recommendations | Supporting Information

ABSTRACT: Mixed Cr(III)−Fe(III) (hydr)oxides ($Cr_xFe_{1-x}(OH)_3$) are common reduction products of Cr(VI) that have long been considered as the sink of Cr in subsurface environments. While current field and laboratory studies have demonstrated that natural organic matter (NOM_{ox}) can dissolve $Cr_xFe_{1-x}(OH)_3$ under oxic conditions, much less is known regarding the dissolution of $Cr_xFe_{1-x}(OH)_3$ by reduced NOM (NOM_{red}) and geochemical behaviors of released Cr(III) under anoxic conditions, which limited our ability to completely predict the cycle of Cr. This study provided new knowledge regarding the simultaneous dissolution of $Cr_xFe_{1-x}(OH)_3$ and formation of Cr(III)-NOM-Fe colloids by NOM_{ox} and NOM_{red} under oxic and anoxic conditions. We showed that NOM dissolved $Cr_xFe_{1-x}(OH)_3$ via ligand-promoted dissolution under oxic conditions and reductive dissolution under anoxic conditions, releasing aqueous Cr(III) and Fe(III/II). Size fractionization results showed that the aqueous Cr(III) and Fe observed at high NOM concentration were Cr(III)-NOM-Fe colloids (ca. 3−450 nm). Dynamic light scattering results further revealed that the colloids had a particle size ranging from 79 to 167 nm and strongly negative surface charges (−40−−17 mV). Cryogenic X-ray photoelectron spectroscopy and X-ray absorption fine structure measurements further indicated a close association of NOM with Cr and Fe within the particle structure. This study provides insights into the fate of $Cr_xFe_{1-x}(OH)_3$ in redox-dynamics and organic-rich environments, which is critical for evaluating the long-term stability of Cr remediation sites.

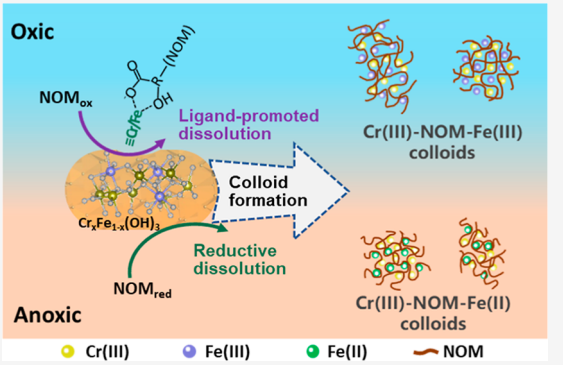

KEYWORDS: *$Cr_xFe_{1-x}(OH)_3$ precipitates, NOM, ligand-promoted dissolution, reductive dissolution, Cr(III)-NOM-Fe colloids, colloid characterization*

1. INTRODUCTION

Chromium (Cr) is an important priority metal pollutant that ubiquitously occurs in subsurface environments and can pose a threat to water quality and human health.[1−3] Under natural conditions, Cr generally exists as either trivalent [Cr(III)] or hexavalent [Cr(VI)] species. Cr(VI), which typically forms oxyanions ($HCrO_4^-$ and CrO_4^{2-}), is toxic and highly mobile.[4,5] In contrast, Cr(III) is less toxic and can form insoluble hydroxide precipitates under neutral conditions.[4,6] Reduction of soluble Cr(VI) to relatively immobile Cr(III) with Fe(II)-based reductants has thus been considered as a promising strategy to constrain the bioavailability of Cr and prevent the spread of contaminant in subsurface environments.[7−12] Due to the similar ionic radii of Cr(III) (61.5 pm) and Fe(III) (64.5 pm)[13,14] and the overwhelming prevalence of iron (hydr)oxides in nature,[15] the mixed Cr(III)−Fe(III) (hydr)oxides ($Cr_xFe_{1-x}(OH)_3$) ($0 < x < 1$) are the common Cr(VI) reduction products that typically serve as the ultimate sink of Cr.[16−19] $Cr_xFe_{1-x}(OH)_3$ precipitates have a lower solubility compared to pure $Cr(OH)_3$. For example, the dissolved Cr(III) in equilibrium with $Cr_xFe_{1-x}(OH)_3$ is 1−5 orders of magnitude lower than the solubility of pure $Cr(OH)_3$ at the same pH.[20] Understanding the chemical stability of $Cr_xFe_{1-x}(OH)_3$ precipitates is therefore of great importance for predicting the long-term remediation efficiency of Cr(VI) in both natural and engineered settings.

Natural organic matter (NOM) is a mixture of redox-active organic macromolecules that can affect the solubility, transport, and toxicity of $Cr_xFe_{1-x}(OH)_3$ precipitates in groundwater and sediments.[21,22] Functional groups of NOM have been found to be capable of dissolving $Cr_xFe_{1-x}(OH)_3$ precipitates via the ligand complexation mechanism,[23−25] in which the chelating moieties (e.g., carboxyl, phenolate, and hydroxamates) form stable metal complexes [complexation constant as high as

Received: August 17, 2022
Revised: October 10, 2022
Accepted: November 18, 2022
Published: November 30, 2022

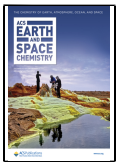

$10^{32.2}$ toward Fe(III) and $10^{30.6}$ toward Cr(III)] that solubilize $Cr_xFe_{1-x}(OH)_3$ precipitates, leading to the release of Cr(III) and Fe(III) ions.[15,23,25] The released Cr(III) and Fe(III) ions can be subsequently bound to NOM as monomeric or polynuclear NOM-Fe(III)−Cr(III) complexes.[26] Myriad field studies also substantiated the elevated aqueous Cr(III) concentrations that are much higher than the solubility of $Cr(OH)_3$ in organic-rich water,[27−31] pointing to an important role played by NOM on the fate and transport of Cr(III) on subsurface.

Although numerous research studies have provided valuable insights into the solubilization of $Cr_xFe_{1-x}(OH)_3$ precipitates by NOM, most prior studies have focused on the effect of oxidized NOM (NOM_{ox}) under oxic conditions.[24,25] To the best of our knowledge, there is limited work devoted to delineating the influence of reduced NOM (NOM_{red}) on the geochemical behavior of $Cr_xFe_{1-x}(OH)_3$ precipitates under anoxic conditions. NOM can exist either as an oxidized or a reduced state in redox dynamic environments.[32] Under anoxic conditions, NOM can be reduced either by microorganisms (e.g., iron-reducing, sulfate-reducing, and fermenting bacteria) or by geochemical reducing species such as sulfide and Fe(II).[33] NOM_{red} exhibits a strong reducing capability (−418 mV, calculated by Eh^0 of the H_2/H^+ redox couple at pH 7) that can reduce a range of redox active transition metals (e.g., Cr, Fe, and Mn) and organic pollution (e.g., nitrobenzenes and chlorinated aliphatic pollutants) under anoxic conditions.[34−39] For example, NOM_{red} can transfer electron from semiquinone or hydroquinone-like moieties to Fe(III) (hydr)oxides, promoting the reductive dissolution of Fe(III) (hydr)-oxides.[34,40] Furthermore, a recent work showed that NOM_{red} can quickly reduce soluble Cr(VI) to Cr(III) that is subsequently complexed with carboxyl groups under anoxic conditions.[33] While the current body of research delineating the redox interactions of NOM_{red} with Fe and Cr alone is acknowledged, the role of NOM_{red} on the dissolution and transformation of $Cr_xFe_{1-x}(OH)_3$ precipitates is rarely explored.

Dissolution of $Cr_xFe_{1-x}(OH)_3$ precipitates by NOM can result in organically complexed metals that remain in aqueous solution. These organically complexed metals have traditionally been regarded as the dissolved phase using a filter membrane (450 or 220 nm pore size), as recommended by U.S. Environmental Protection Agency (EPA) for dissolved metal determination. Nevertheless, recent advances reported that organically complexed metals [e.g., Cr(III)-NOM-Fe(III)] can be presented as colloids with size ranging from ca. 3 to 450 nm.[26,41,42] NOM-Cr(III) colloids play critical roles in the fate and transport of Cr(III) on the subsurface. For example, the high mobility of NOM-Cr(III) colloids in the subsurface can increase the likelihood of their interactions with Mn(IV)-containing minerals, which poses a threat of reoxidation of Cr(III) to Cr(VI).[43−45] Therefore, it is of great importance to have a detailed understanding of the formation and properties of NOM-Cr(III) colloids to evaluate their impact on the chemical stability of reduced Cr(III) products.

The objective of this study was to investigate the dissolution of $Cr_xFe_{1-x}(OH)_3$ precipitates and the formation of Cr(III)-NOM-Fe colloids using NOM of different redox states under both oxic and anoxic conditions. To this end, wet chemical analysis was used to monitor the dissolution kinetics of $Cr_xFe_{1-x}(OH)_3$ and the formation of Cr(III)-NOM-Fe colloids. Dynamic light scattering (DLS), X-ray photoelectron spectroscopy (XPS), and X-ray absorption fine structure (XAFS) analysis were collectively used to yield insights into the properties of Cr(III)-NOM-Fe colloids. Results gained from this study advance our understanding of the long-term stability of the Cr remediation site in organic-rich environments.

2. MATERIALS AND METHODS

2.1. $Cr_xFe_{1-x}(OH)_3$ Synthesis and Characterization. $Cr_xFe_{1-x}(OH)_3$ precipitates were synthesized following previously established methods.[25,46] Briefly, $Cr(NO_3)_3{\cdot}9H_2O$ and $Fe(NO_3)_3{\cdot}9H_2O$ were dissolved in ultrapure water (resistivity >18.2 MΩ·cm, Millipore) to yield a total metal concentration of 100 mM with desired Fe/Cr molar ratios of 1:0, 4:1, 1:1, 1:4, and 0:1. The suspensions were then titrated to pH 7 ± 0.2 with 1 M NaOH solution, followed by washing several times with ultrapure water until the conductivity <200 μS/cm. The synthesized precipitates, namely $Cr(OH)_3$, $Cr_{0.8}Fe_{0.2}(OH)_3$, $Cr_{0.5}Fe_{0.5}(OH)_3$, $Cr_{0.2}Fe_{0.8}(OH)_3$, and $Fe(OH)_3$, were characterized by powder X-ray diffraction (XRD, Bruker D8 Advance). XRD patterns of the $Cr_xFe_{1-x}(OH)_3$ at high Fe/Cr ratios (x = 0.2) appeared similar to that of 2-line ferrihydrite (broad peaks at 35 and 63° 2θ for Cu Kα) and without the characteristic peak of $Cr(OH)_3$ at 2θ = 19.1° (Figure S1, Supporting Information), which was in line with previous reports.[20,47−49] With increase in the Cr content (x = 0.5 and 0.8), the characteristic peak of $Cr(OH)_3$ increased and eventually evolved into $Cr(OH)_3$ (x = 1). The Brunauer−Emmett−Teller (BET) surface area was determined with a Micromeritics surface area analyzer (ASAP-2020) using N_2 adsorption at 77 K. The determined BET surface areas were 223.4 m^2/g for $Fe(OH)_3$, 244.2 m^2/g for $Cr_{0.2}Fe_{0.8}(OH)_3$, 77.3 m^2/g for $Cr_{0.5}Fe_{0.5}(OH)_3$, 322.0 m^2/g for $Cr_{0.8}Fe_{0.2}(OH)_3$, and 100.2 m^2/g for $Cr(OH)_3$. The synthesized $Cr_xFe_{1-x}(OH)_3$ precipitates were stored in the dark at 4 °C prior to use.

2.2. NOM Isolation and Characterization. Aldrich humic acid (AHA, 1415-93-6, Sigma-Aldrich) was chosen as a representative of NOM, owing to its well-characterization and wide application in colloid chemistry research.[33,42,50,51] The AHA stock solution was prepared by dissolving aliquots of dried powder in 1 L ultrapure water at pH 10.5 ± 0.1 in the dark with constant stirring. After 3 days of rotation, the AHA suspension was filtered through 450 nm nitrocellulose membranes (Millipore). The filtrate solution was referred to as oxidized AHA (AHA_{ox}). To emulate the AHA with reduced redox state under anoxic conditions, an aliquot of the AHA_{ox} solution was then chemically reduced using 5% H_2 in the presence of a Pd catalyst (5% wt on Al_2O_3 spheres, 1 g/L, Sigma-Aldrich) in an anoxic glovebox (95% N_2 and 5% H_2, Coy Laboratory Products Inc., MI), as described in our previous studies.[26,50,52] The resulting suspension was accordingly referred to as reduced AHA (AHA_{red}). The stock AHA solutions were wrapped with aluminum foil to prevent any potential photoreaction and were stored in the anoxic glovebox for further use. The concentrations of AHA_{ox} and AHA_{red} stock suspensions were determined using a total organic carbon (TOC) analyzer (Multi N/C 3100, Analytik Jena).

2.3. Batch Experiments. All batch experiments were conducted at room temperature (25 ± 0.5 °C) using 50 mL polypropylene vials that were continuously stirred with magnetic stir bars and shielded with aluminum foil (see experimental conditions in Table S1). All the reaction suspensions contained a background NaCl concentration of

https://doi.org/10.1021/acsearthspacechem.2c00255
ACS Earth Space Chem. 2022, 6, 2995−3006

5 mM as the electrolyte solution and were buffered at pH 6 with 10 mM 2-morpholinoethansulfonic acid monohydrate (MES, Sigma-Aldrich). MES was selected because it neither complexes with metal ions nor participates in redox reactions with Cr and Fe.[3,42] The experiments of $Cr_xFe_{1-x}(OH)_3$ dissolution under the influence of AHA_{red} were conducted under anoxic conditions in an anoxic glovebox ($P_{O2} < 10^{-6}$ bar),[53] and the dissolved oxygen (DO) concentration in the well-mixed suspensions was always below the detection limit of 0.01 mg/L, as measured by the DO probe (HACH). Accordingly, the dissolution experiments under the influence of AHA_{ox} were conducted under oxic conditions (P_{O2} = 0.21 bar) in the open air, and the DO concentration reached saturation (~8.2 mg/L) within 1 h of exposure to the air.

For the anoxic experiments performed in the anoxic glovebox, all the solution preparation and oxygen-sensitive procedures were conducted inside the glovebox. The synthesized $Cr_xFe_{1-x}(OH)_3$ precipitates were added into the suspension to reach a final Cr and Fe concentration of 1 mM. Aliquots of the AHA_{red} stock solution were then spiked into the abovementioned suspensions to a final concentration of 50 ± 1 or 170 ± 2 mg C/L to initiate the reaction. For the oxic experiments, the ultrapure water used for solution preparation was sparged with air for ≥12 h. Oxic experiments were initiated by mixing 1 mM of synthesized $Cr_xFe_{1-x}(OH)_3$ precipitate suspension with 50 ± 1 and 170 ± 2 mg C/L of AHA_{ox} under oxic conditions. Control experiments were performed with addition of $Cr_xFe_{1-x}(OH)_3$ precipitates but in the absence of AHA in the abovementioned reaction suspensions under oxic conditions. To monitor the process of the reaction, aliquot samples were periodically collected from the suspensions throughout the timeframe of the experiments. All batch experiments were conducted at least in duplicate.

2.4. Analytical Techniques. Aqueous samples were filtered through 220 nm membrane (PES, Millipore), and the filtrate was analyzed immediately for total aqueous Cr, aqueous Fe(II), and total aqueous Fe [including Fe(II) and Fe(III)]. The samples for total Cr and Fe analysis were acidified with 6% HNO_3 and stored at 4 °C in the dark prior to analysis. Total aqueous Cr and Fe concentrations were determined using Agilent 7700 series inductively coupled plasma mass spectrometry. Total Fe(II) was determined after digesting the unfiltered samples in 1 M HCl for 24 h at room temperature in the dark. During the acidic incubation period, the AHA precipitated and was further removed through centrifugation (14,000*g* for 10 min).[50,54] Furthermore, fluoride was added initially to the sample to suppress the potential Fe(III) reduction by AHA and to prevent the formation of colored Fe(III)-phenanthroline complexes.[52] The total and aqueous Fe(II) were measured spectrophotometrically using a modified 1,10-phenanthroline method.[55] The aqueous Fe(III) concentration was calculated by subtracting the aqueous Fe(II) concentration from the total aqueous Fe concentration.

At the end of each experiment, aliquots of suspensions were sequentially filtrated through 220 nm membranes (PES, Millipore) and 10 kDa ultrafiltration membranes (ca. 3 nm, EMD, Millipore). The filtrate through a 10 kDa membrane pointed to the truly dissolved (<ca. 3 nm) species. Accordingly, the colloidal fraction (ca. 3−220 nm) was defined as the difference between the filtrate through 220 nm and the filtrate through 10 kDa membrane. DLS (Zetasizer Nano, Malvern) was employed to measure the particle size distribution and zeta potential of the aqueous samples. Selected solid samples were collected at the end of batch experiments, followed by centrifugation and freeze-drying under anoxic conditions. Surface properties of the resulting solids were characterized by cryogenic XPS performed at −160 °C. To study the vertical distribution of Cr, Fe, and NOM, a XPS depth profiling technique was employed to etch samples from sample near-surface to 100 nm depth using an argon gun operating at 2 kV. XPS spectra were collected using a PHI Quantera SXM scanning X-ray microprobe with an Al mono source at a 100 μm X-ray spot size. The binding energies were calibrated using C 1s at 284.8 eV, and the spectra were proceeded using MultiPak v9.8 software. Cr and Fe K-edge X-ray absorption near edge structure (XANES) and extended X-ray absorption fine structure (EXAFS) spectra were collected in the fluorescence mode on the beamline 20BM at the advanced photon source (APS), Argonne, USA. Three to six scans were performed for each sample. The detailed description of XAFS analysis was reported previously;[56,57] a summary is also provided in Section S1 of Supporting Information.

3. RESULTS AND DISCUSSION

3.1. NOM-Induced Dissolution of $Cr_xFe_{1-x}(OH)_3$ under Oxic and Anoxic Conditions. Control experiments without AHA show negligible dissolution of $Cr_xFe_{1-x}(OH)_3$ precipitates. The concentration of aqueous Cr(III) from $Cr(OH)_3$ was 1−2 μM after 72 h of dissolution at pH 6, while aqueous Cr(III) from Fe-containing precipitates was below the detection limit of 0.2 μM. This is in agreement with previous reports that Fe−Cr coprecipitation can lower the dissolution of Cr (hydr)oxides.[48,58] The Fe-containing $Cr_xFe_{1-x}(OH)_3$ precipitates are mainly in the form of ferrihydrite (Figure S1), which is also consistent with previous studies,[20,59] exhibiting a smaller solubility product (K_{sp} = 2.8 × 10^{-39}, 298 K) than that of $Cr(OH)_3$ (K_{sp} = 6 × 10^{-31}, 298 K).

The results from the batch experiments indicated that NOM promoted the dissolution of $Cr(OH)_3$ (Figure 1a). The aqueous Cr concentrations from $Cr(OH)_3$ were ~30 μM at 50 mg C/L AHA under both oxic and anoxic conditions. With the AHA concentration elevated to 170 mg C/L, the aqueous Cr(III) concentrations were ~61 μM for AHA_{ox} under oxic concentration and ~90 μM for AHA_{red} under anoxic conditions. While the reactive oxygen species (ROS) can be produced from oxygenation of reduced NOM by molecular oxygen,[52,60−62] the ROS production was unlikely to occur in this study because the reduced AHA was reacted in the absence of oxygen. Therefore, the redox reaction between $Cr(OH)_3$ and AHA is lacking. Thus, the generation of aqueous Cr(III) is likely through a ligand-promoted dissolution mechanism, which is an effective pathway that can accelerate dissolution of metal (hydr)oxides through ligand complexation with surface metal atoms and the subsequent detachment of the metal complex.[15,63,64] Because $Cr(OH)_3$ is positively charged at pH 6 (Figure S2), the negatively charged functional groups (e.g., carboxylic, alcoholic, and quinone) of AHA_{red} are more readily adsorb on the surface of $Cr(OH)_3$ via electrostatic interactions, thus enhancing the complexation dissolution and producing aqueous Cr(III).

The presence of NOM also promoted the dissolution of $Cr_xFe_{1-x}(OH)_3$ precipitates, but the released amount of aqueous Cr(III) was much smaller than those from pure $Cr(OH)_3$ (Figure 1b−d). Irrespective of the oxic and anoxic conditions, the aqueous Cr(III) concentrations increased with

https://doi.org/10.1021/acsearthspacechem.2c00255
ACS Earth Space Chem. 2022, 6, 2995−3006

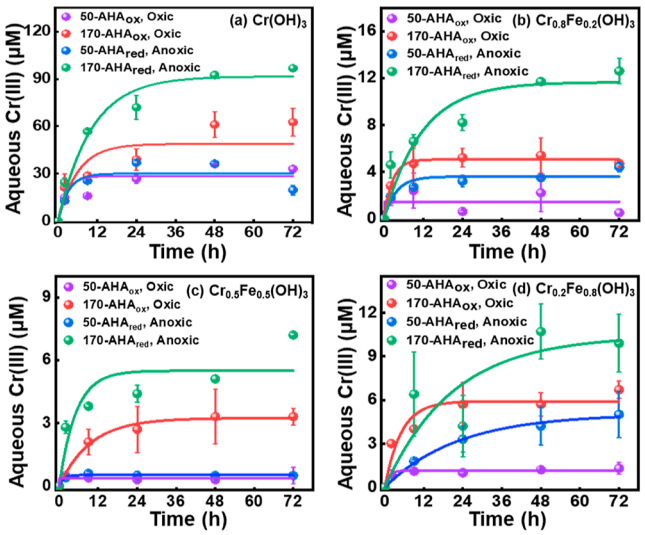

Figure 1. Evolution of aqueous Cr(III) from $Cr_xFe_{1-x}(OH)_3$ precipitates under the influence of AHA with varying concentrations and redox states under oxic and anoxic conditions at pH 6. The legends of 50-AHA_{ox}, oxic and 170-AHA_{ox}, oxic indicated that the dissolution of $Cr_xFe_{1-x}(OH)_3$ were conducted in the presence of 50 mg C/L AHA_{ox} and 170 mg C/L AHA_{ox} under oxic conditions. The legends of 50-AHA_{red}, anoxic and 170-AHA_{red}, anoxic indicate that the dissolution of $Cr_xFe_{1-x}(OH)_3$ was conducted in the presence of 50 mg C/L AHA_{red} and 170 mg C/L AHA_{red} under anoxic conditions. The aqueous Cr(III) concentration was determined after filtration through a 220 nm PES syringe filter. Solid lines represent the pseudo-first-order model fits using equation $C_t = C_{eq}\cdot(1 - e^{-kt})$, where C_t and C_{eq} are the aqueous Cr(III) concentration at time t and equilibrium, respectively. Please note that the pseudo-first-order model was just used to simply evaluate the aqueous Cr(III) concentrations and to guide the eyes. Error bars represent the standard deviations of at least duplicate measurements. Where error bars are not visible, they are smaller than the data symbols.

increasing AHA concentration. Interestingly, the aqueous Cr(III) concentrations observed under anoxic conditions were 1.5−2 times higher than those observed under oxic conditions at the same AHA concentration. For example, after 72 h of the reaction at high AHA concentration (170 mg C/L), the aqueous Cr(III) concentrations from $Cr_{0.5}Fe_{0.5}(OH)_3$ are approximately 5.5 μM under anoxic conditions and 3.2 μM under oxic conditions (Figure 1c). This is predominately due to the fact that AHA_{red} reduced structural Fe(III) in $Cr_xFe_{1-x}(OH)_3$ precipitates via a reductive dissolution mechanism, which led to the release of Cr(III) and Fe(III/II) into the aqueous phase (Figure 2). Similar observations of the reductive dissolution of iron minerals (e.g., ferrihydrite, goethite, and hematite) by chemically reduced NOM have been previously reported.[40,64,65] In contrast, under oxic conditions, AHA_{ox} dissolved $Cr_xFe_{1-x}(OH)_3$ mainly via ligand-promoted dissolution,[25,46] which was not as significant as reductive dissolution using AHA_{red} under anoxic conditions. No significant difference in Cr(III) dissolution was observed from different Fe-containing $Cr_xFe_{1-x}(OH)_3$ precipitates under both oxic and anoxic conditions, which might be attributed to the changes in physiochemical properties of $Cr_xFe_{1-x}(OH)_3$ caused by varying initial Fe/Cr molar ratios. Previous research studies have reported that the initial Fe/Cr molar ratio of $Cr_xFe_{1-x}(OH)_3$ precipitates affects their structural and surface atom arrangements.[48,59,66] Specifically, increasing Fe contents increased the crystallinity of synthesized $Cr_xFe_{1-x}(OH)_3$ precipitates (Figure S1), which may decrease the electron-accepting capability of $Cr_xFe_{1-x}(OH)_3$ toward AHA.[15,67,68] In contrast, increasing Fe contents might enhance the interaction of Fe(III) with reducing functional groups (i.e., quinone-like moieties) of AHA, thus promoting the reduction of Fe(III) to Fe(II). Therefore, the overall effect of the Fe/Cr molar ratio of the $Cr_xFe_{1-x}(OH)_3$ precipitate was not significant on NOM-induced dissolution under the conditions tested.

The generation of aqueous Fe(III) resulted from ligand-promoted dissolution,[25,64] and the generation of Fe(II) from $Cr_xFe_{1-x}(OH)_3$ indicated the reduction of structural Fe(III) by AHA (Figures 2 and S3).[40,69] Under oxic conditions, only aqueous Fe(III) was detected. With 50 mg C/L AHA_{ox}, the aqueous Fe(III) from $Cr_{0.8}Fe_{0.2}(OH)_3$ and $Cr_{0.5}Fe_{0.5}(OH)_3$ reached approximately 2.8 μM after 72 h of reaction (Figure 2a,b). A high aqueous Fe(III) concentration was observed at a higher molar Fe/Cr ratio (i.e., $Cr_{0.2}Fe_{0.8}(OH)_3$) and a high AHA concentration of 170 mg C/L (Figure 2c,d). Under anoxic conditions, Fe(II) was generated (Figure 2e−h). For all Fe-containing precipitates, the concentration of total Fe(II) ranged from 60 to 80 μM at 50 mg C/L AHA_{red} and increased greatly up to 190−220 μM at 170 mg C/L AHA_{red} (Figure S3). The great increase in Fe(II) suggests that reductive dissolution played an important role in the dissolution of Fe-containing precipitates. The aqueous Fe(III) concentration across all Fe-containing precipitates was only 2−5 μM at 50 mg C/L AHA_{red} and was not detected at 170 mg C/L AHA_{red} (data not shown) (Figure 2a−d). The absence of aqueous Fe(III) at high AHA_{red} concentration may be attributable to the fact that the intermediate aqueous Fe(III) was subsequently reduced to Fe(II) by free reducing moieties of AHA_{red}.[41] Taken together, ligand-promoted dissolution and reductive dissolution of Fe(III) under anoxic conditions collectively contributed to the dissolution of aqueous Fe from $Cr_xFe_{1-x}(OH)_3$.

Regardless of the oxic and anoxic conditions, more aqueous Fe(III/II) was dissolved from $Cr_xFe_{1-x}(OH)_3$ than aqueous Cr(III) for a given Fe/Cr ratio (Figures 1 and 2). The ratios of aqueous Fe/Cr to inherent molar Fe/Cr ratio ($[Fe/Cr]_{aq}/[Fe/Cr]_{in}$) were typically >1 (Figure S4), indicating that more aqueous Fe was released than Cr(III). The preferential release of Fe over Cr is consistent with previous report showing that the dissolution of $Cr_xFe_{1-x}(OH)_3$ by siderophore and organic acid resulted in more Fe released with enrichment of Cr in the residual solid phase.[25] Taken as a whole, under both oxic and anoxic conditions, NOM solubilized $Cr_xFe_{1-x}(OH)_3$ precipitates via ligand-promoted dissolution mechanism and reductive dissolution mechanism and released more aqueous Fe(III/II) than Cr.

3.2. Formation of Cr(III)-NOM-Fe Colloids. Dissolution of $Cr_xFe_{1-x}(OH)_3$ precipitates by NOM is accompanied by the formation of Cr(III)-NOM-Fe colloids. Since the concentrations of aqueous Cr(III) (>12 μM, Figure 1a) observed at the end of the batch experiments were appreciably higher than the predicted solubility of $Cr(OH)_3$, which is 0.6 μM under the studied conditions, a subset of aqueous samples were further passed through an ultrafiltration membrane with a 10 kDa cutoff (ca. 3 nm) to identify the contribution of colloidal particles to the aqueous concentrations. Control experiments without NOM show that the truly dissolved Cr(III) concentrations (<0.2 μM) were consistently below the expected solubility of $Cr(OH)_3$. With NOM present, the

https://doi.org/10.1021/acsearthspacechem.2c00255
ACS Earth Space Chem. 2022, 6, 2995−3006

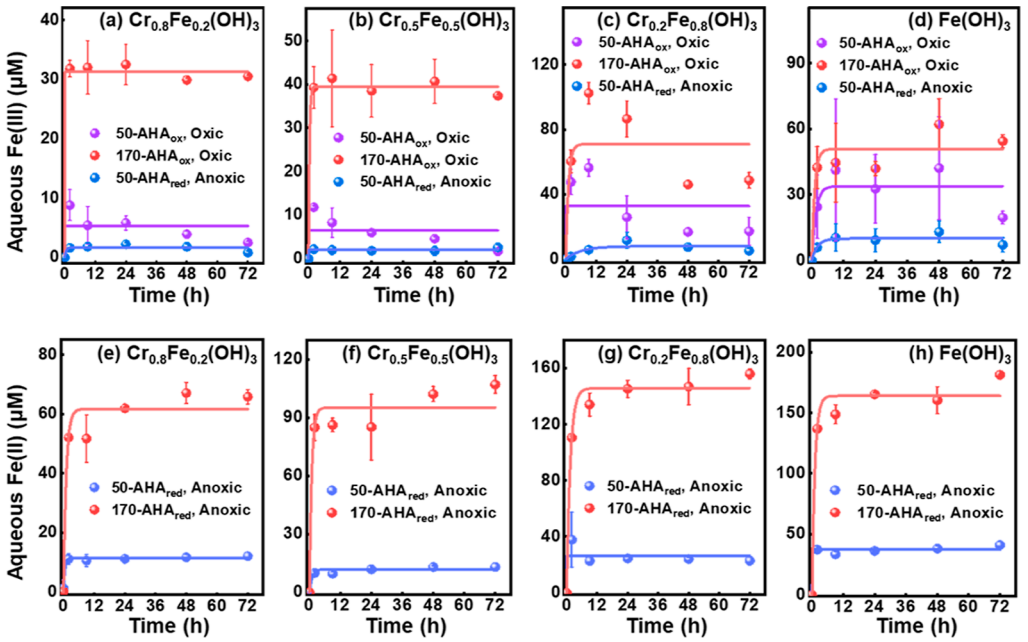

Figure 2. Generation of (a–d) aqueous Fe(III) and (e–h) aqueous Fe(II) from $Cr_xFe_{1-x}(OH)_3$ precipitates in the presence of AHA under oxic and anoxic conditions at pH 6. The aqueous Fe concentration was determined after filtration through a 220 nm PES syringe filter. Aqueous Fe(III) measured at 170 mg C/L AHA_{red} was below the detection limit of instrument and not detected; therefore, it was not plotted. The legends of 50-AHA_{ox}, oxic and 170-AHA_{ox}, oxic indicate that the dissolution of $Cr_xFe_{1-x}(OH)_3$ was conducted in the presence of 50 mg C/L AHA_{ox} and 170 mg C/L AHA_{ox} under oxic conditions; the legends of 50-AHA_{red}, anoxic and 170-AHA_{red}, anoxic indicate that the dissolution of $Cr_xFe_{1-x}(OH)_3$ was conducted in the presence of 50 mg C/L AHA_{red} and 170 mg C/L AHA_{red} under anoxic conditions. Solid lines represent the pseudo-first-order model fits using the equation $C_t = C_{eq}\cdot(1 - e^{-kt})$, where C_t and C_{eq} are the aqueous Fe(III/II) concentration at time t and equilibrium, respectively. Please note that the pseudo-first-order model was just used to simply evaluate the aqueous Fe(III) and Fe(II) concentrations and to guide the eyes. Error bars represent the standard deviations of at least duplicate measurements. Where error bars are not visible, they are smaller than the data symbols.

colloidal Cr(III) (ca. 3–220 nm) accounted for up to 76–97% of the aqueous Cr(III) released from $Cr_xFe_{1-x}(OH)_3$ precipitates under both oxic and anoxic conditions (Figure 3a). In addition to Cr, almost all the aqueous Fe were colloidal Fe(III) under oxic conditions (Figure 3b). Under anoxic conditions, the truly dissolved Fe(II) made up to 32–72% of the aqueous Fe at 50 mg C/L AHA_{red}, while the colloidal Fe(II) accounted for 86–89% of aqueous Fe when elevating AHA_{red} concentration to 170 mg C/L (Figure 3b). Compared to Cr(III) and Fe(III), the relatively high fraction of truly dissolved Fe(II) at low NOM concentration may be ascribed to the high solubility of $Fe(OH)_2$ at pH 6 ($K_{sp} = 4.9 \times 10^{-17}$, 25 °C). Additionally, the complexation constant of Fe(II)-NOM complexes is 2–4 orders of magnitude lower than that of Fe(III)-NOM complexes (log $K_{Fe(II)}$ = 5.4–10.2 versus log $K_{Fe(III)}$ = 9.5–12.9),[70,71] allowing Fe(II) to exist as truly dissolved phases at a low NOM loading. At high NOM concentration, the similar colloidal behaviors between Cr(III) and Fe(III/II) suggest their close associations in colloidal fractions during the NOM-induced dissolution of $Cr_xFe_{1-x}(OH)_3$ precipitates. The formation of Cr(III)-NOM-Fe colloids is dominantly owing to the complexation of Cr(III) and Fe with NOM, which inhibits the hydrolysis of Cr(III) and Fe ions and thus favors the smaller particle sizes.[21,50,51,72,73]

Particle size and zeta potential measured by DLS support the dispersion of Cr(III)-NOM-Fe colloids. The hydrodynamic diameters of Cr(III)-NOM-Fe colloids formed under both oxic and anoxic conditions ranged from 79 to 167 nm (Figure 4a). The zeta potential results show that Cr(III)-NOM-Fe colloids possessed strongly negative surface charges (i.e., −40−−17 mV, Figure 4b), further ensuring the particle stability of colloids. Under anoxic conditions, the particles have a higher surface negative charge compared to the particles formed under oxic conditions, which may be ascribed to the more reduced functional groups in AHA_{red} than AHA_{ox}.[32,33,38,39] Altogether, the stability of Cr(III)-NOM-Fe colloids formed under both oxic and anoxic conditions can be attributable to the enhanced electrostatic and steric stabilization imparted by NOM adsorbed on the particle surfaces.[26,51,74]

3.3. Characterization of Cr(III)-NOM-Fe Colloids and Large Particles. Cryogenic XPS spectroscopy analysis in conjunction with depth profiles identified the chemical state and distribution of Cr and Fe present at the near surface of the particles. Because the Cr(III)-NOM-Fe colloids formed for all conditions examined, cryogenic XPS measurements were only performed in the samples of $Cr_{0.8}Fe_{0.2}(OH)_3$ before and after reactions with AHA_{ox} and AHA_{red} under both oxic and anoxic conditions (Figure 5). The high-resolution Cr 2p spectra show that only Cr(III) characteristic peaks ranging from 576.2 to 579.0 eV were observed for all conditions with no significant Cr(VI) peaks at ~579.4 eV[44,68] (Figure 5a–d). This indicates that neither AHA_{ox} nor O_2 oxidized Cr(III) to Cr(VI) within the timescale of the experiments, which is consistent with other reports under the similar experimental conditions.[44,75] High-resolution Fe 2p spectra indicated that Fe was present as Fe(III) under oxic conditions (Figure 5e,f). A weak peak of Fe(II) (708.0 eV)[76–78] was observed under anoxic conditions at high NOM concentration but was absent at low NOM concentration (Figure 5g,h) due to the relatively lower Fe(II) generation. Such observation is in agreement with wet

https://doi.org/10.1021/acsearthspacechem.2c00255
ACS Earth Space Chem. 2022, 6, 2995−3006

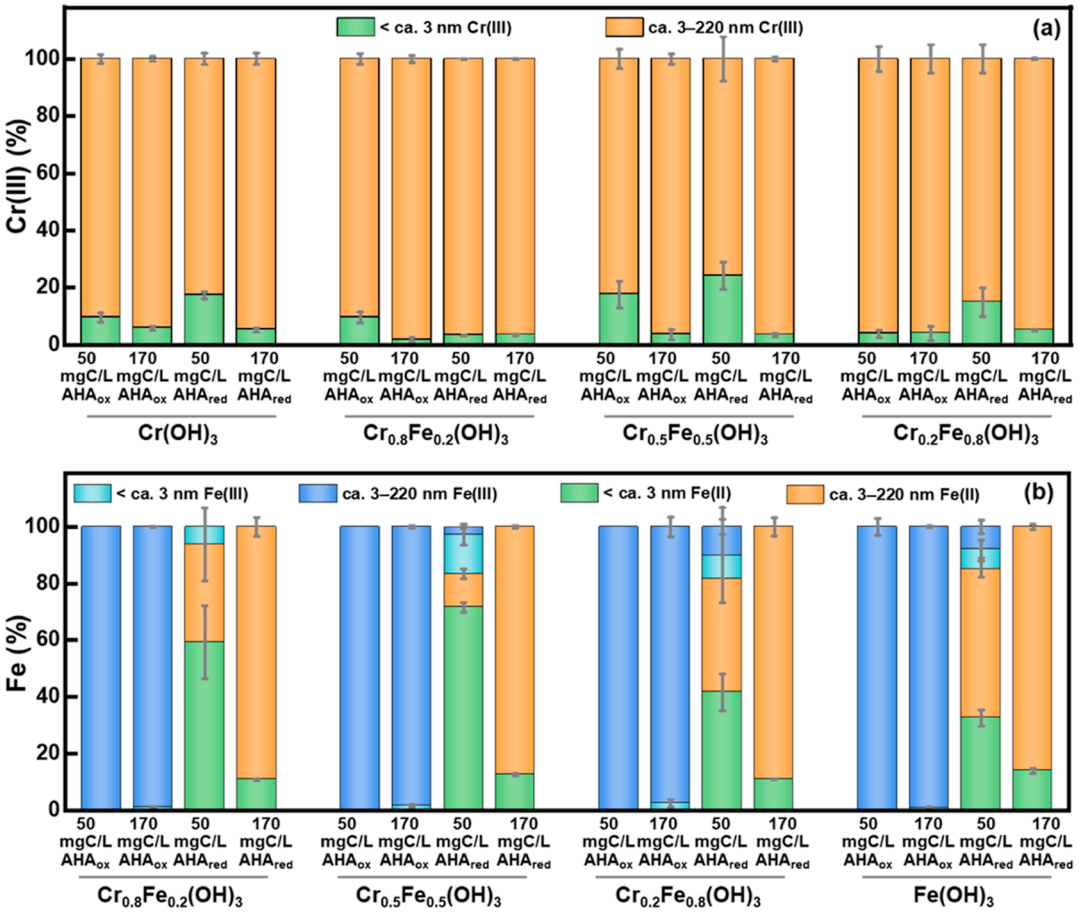

Figure 3. Percentage of (a) Cr(III) and (b) Fe, including Fe(II) and Fe(III), in different size fractions collected after 72 h of reaction of $Cr_xFe_{1-x}(OH)_3$ precipitates (x = 0, 0.2, 0.5, 0.8, and 1) with AHA (AHA_{ox} and AHA_{red}) under oxic and anoxic conditions at pH 6. The percentage on the y-axis represents the fraction of Cr and Fe in a certain size fraction to their corresponding total concentration of aqueous Cr and Fe through 220 nm membrane. Under oxic conditions, all aqueous Fe was Fe(III). Under anoxic conditions, both Fe(II) and Fe(III) exist at 50 mg C/L AHA_{red}, while only Fe(II) exists at 170 mg C/L AHA_{red}. Error bars represent standard deviations of duplicate measurements.

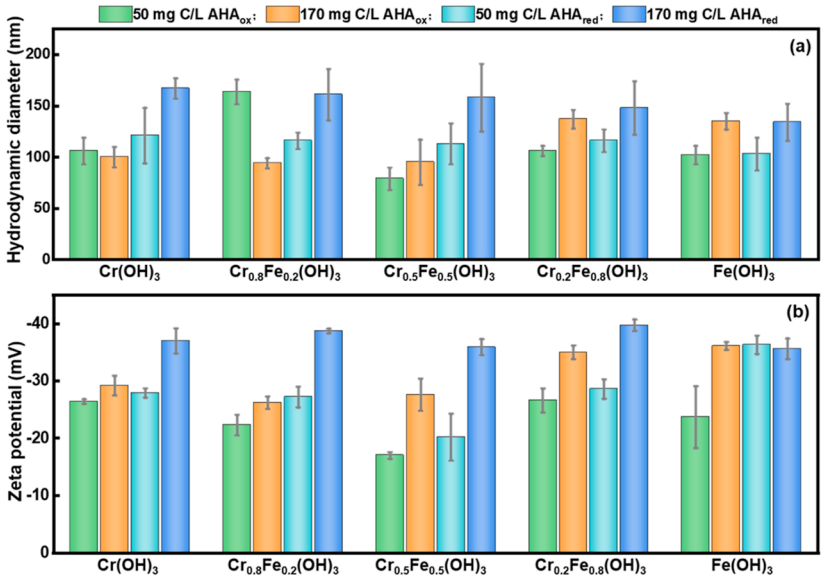

Figure 4. (a) Z-averaged hydrodynamic diameter and (b) zeta potentials of Cr(III)-NOM-Fe colloids collected after 72 h of reactions under oxic and anoxic conditions at pH 6. Error bars represent the standard deviations of at least duplicate measurements.

chemistry results described above (Figure 2). Furthermore, the XPS depth profiling technique provided information on the spatial distribution of Cr, Fe, and NOM as a function of probing depth. Control experiments without NOM show that

https://doi.org/10.1021/acsearthspacechem.2c00255
ACS Earth Space Chem. 2022, 6, 2995−3006

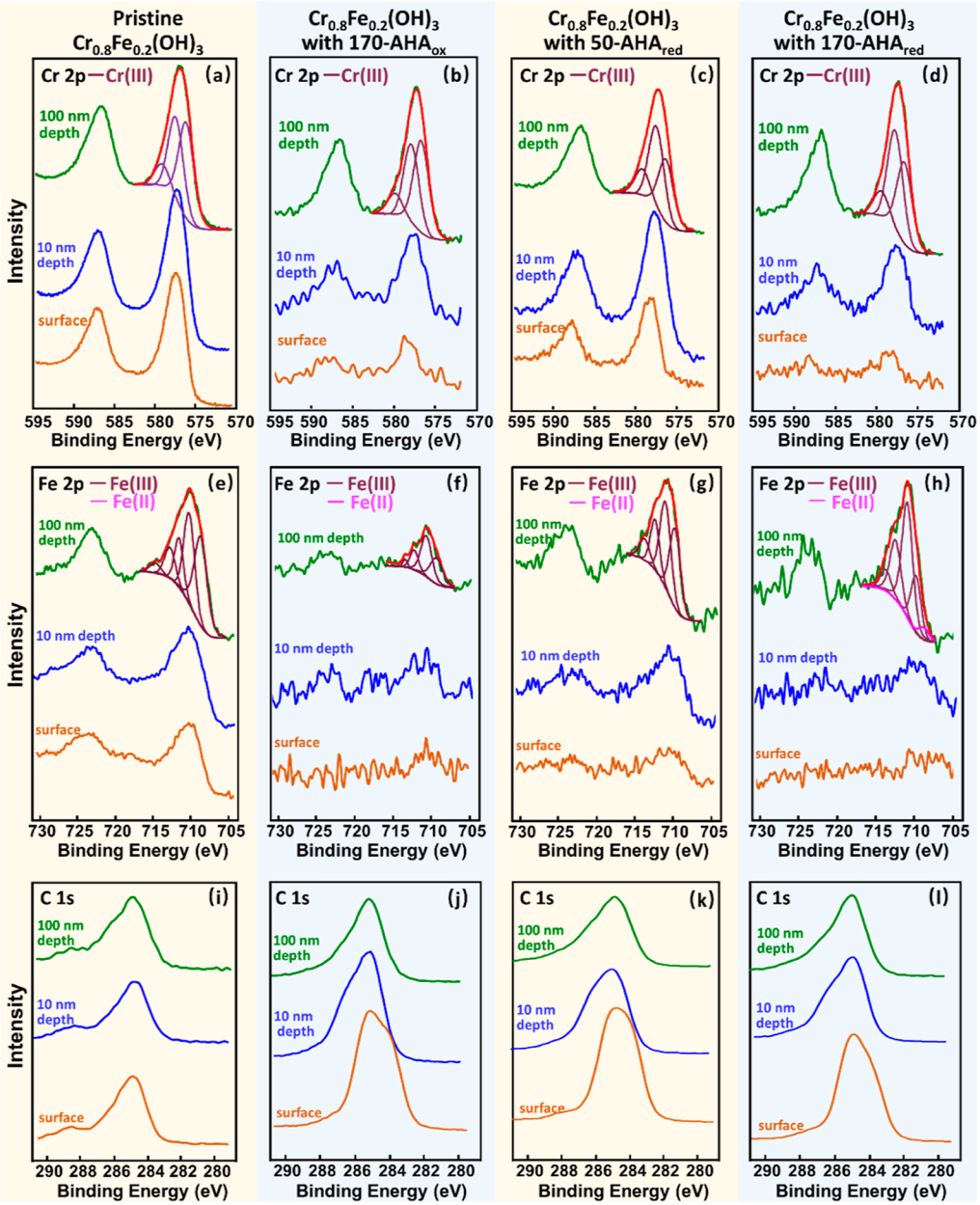

Figure 5. Cryogenic XPS (a–d), Cr 2p, (e–h), and Fe 2p and (i–l) C 1s spectra of (first column) pristine $Cr_{0.8}Fe_{0.2}(OH)_3$ without AHA, and samples collected after 72 h of reaction of $Cr_{0.8}Fe_{0.2}(OH)_3$ with (second column) 170 mg C/L AHA_{ox} under oxic conditions, with (third column) 50 mg C/L AHA_{red}, and with (fourth column) 170 mg C/L AHA_{red} under anoxic conditions at pH 6, respectively. The probing depths were recorded at surface, 10, and 100 nm of samples. Raw data were calibrated to C 1s at a binding energy of 284.8 eV and fitted using a least squares procedure with the Gaussian–Lorentzian function (80% G-20% L) after subtracting a Shirley background. Peak fitting was performed for Cr $2p_{3/2}$ and Fe $2p_{3/2}$ peaks contained at a probing depth of 100 nm, due to the high signal intensity. Peak fittings for Cr $2p_{3/2}$ peaks and Fe $2p_{3/2}$ peaks were assigned based on the literature-reported values.[76−78,94−96]

the intensity of Cr(III) and Fe(III) remained unchanged with increasing probing depth (Figure 5a,e), suggesting the even distribution of Cr(III) and Fe(III) within the tested precipitate (i.e., $Cr_{0.8}Fe_{0.2}(OH)_3$). In stark contrast, with NOM present, the Cr(III) and Fe(III) intensities increased significantly as the probing depth increased from the near-surface to 100 nm depth along the surface (Figure 5b–d,f–h), demonstrating the enrichment of NOM on the surface of Cr(III)-NOM-Fe colloids. This is in part supported by the decreased carbon intensity with increasing probing depth (Figure 5j–l). The enrichment of NOM on the particle surface confirmed the stabilization mechanisms of electrostatic and steric interactions responsible for the enhanced dispersion of Cr(III)-NOM-Fe colloids under conditions tested. Furthermore, inspection of the atom percentages of Cr, Fe, C, and O at different probing depths revealed that the Cr/Fe ratios at the particle near surface are significantly higher than those at depths of 10 and 100 nm (Table S2), indicating a relative enrichment of Cr at the particle surface, which further supports the favorable dissolution of Fe (Figure S4).

XAFS analysis was further used to quantify the speciation and local molecular coordination environments of Cr and Fe within the particle structure. Cr K-edge XANES spectra show that no Cr(VI) is observed in any of the samples, as evidenced

https://doi.org/10.1021/acsearthspacechem.2c00255
ACS Earth Space Chem. 2022, 6, 2995−3006

by the absence of an intense pre-edge peak at ~5993 eV (Figure 6a).[79] The weak pre-edge feature at ~5990 eV, the

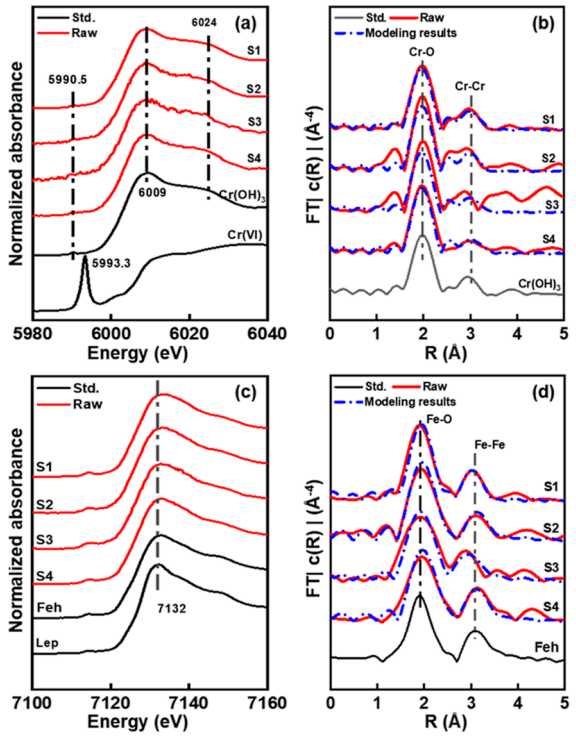

Figure 6. (a,c) K-edge normalized XANES spectra of (a) Cr and (c) Fe; (b,d) Fourier transforms (magnitudes) of the k^3-weighted EXAFS spectra (with phase correction) of (b) Cr and (d) Fe. The red solid line, blue dot-dash line, and black solid line represent raw, modeled, and standard reference compound spectra, respectively. Parameters of the EXAFS modeling are reported in Tables S4 and S5. The reaction samples were collected after 72 h of reactions under oxic and anoxic conditions at pH 6. S1 is referred to as pristine $Cr_{0.8}Fe_{0.2}(OH)_3$; S2, S3, and S4 are referred to as samples obtained from the reaction of $Cr_{0.8}Fe_{0.2}(OH)_3$ with 170 mg C/L AHA_{red}, with 170 mg C/L AHA_{ox}, and with 50 mg C/L AHA_{ox}, respectively. For reference, the patterns of $Cr(OH)_3$, Cr(VI), ferrihydrite (Fh), and lepidocrocite (Lep) are included in the XANES and EXAFS plots.

main peak at 6009 eV, and a shoulder peak at 6024 eV are typical peaks of Cr(III),[80] further confirming that no oxidation of Cr(III) occurred during the experiments (Figure 6a). The linear combination fitting (LCF) results of Cr k^3-weighted EXAFS show that $Cr(OH)_3$ is the only identifiable species of Cr species (Figure S5a and Table S3). The first-shell modeling from the Cr K-edge EXAFS spectra indicated an average Cr−O distance of 1.97 Å with a coordination number of Cr ranging from 5.3 to 5.9 (Figure 6b and Table S3). The measured Cr−O distance indicated that Cr(III) had six coordinating oxygen atoms in an octahedral geometry under the tested conditions.[21,66] The second shell is likely to be Cr−Cr with a distance of 3.02 Å,[81] and the coordination number ranged from 1.4 to 2.2. The smaller coordination numbers (1.4−1.5) of Cr−Cr from AHA-treated samples are likely due to the interference from close complexation with AHA (Figure 6b, Table S3), which would lead to the smaller particle sizes or more structural disorder of Cr(III) within the particle structure, as observed in previous reports.[21,82−84]

Fe K-edge EXAFS spectra provide information on the redox state and local coordination environments of Fe (Figure 6c,d and Table S4). XANES results indicated that only Fe(III) was present (Figure 6c) as characteristic peaks of Fe(III) were located at ~7132 eV, and ferrihydrite was the only identifiable species of Fe species, as evidenced by LCF results of Fe k^3-weighted EXAFS (Figure S5b and Table S4). In general, Fe(III) had six coordinating oxygen atoms in an octahedral geometry with an Fe−O distance of 1.99 Å (Figure 6d and Table S4). The second shell is likely to be Fe−Fe with a distance of 3.01 Å and a coordination number of 3.8 (Figure 6d and Table S4). However, the Fe−Fe of AHA-induced Cr(III)-NOM-Fe colloids has relatively smaller coordination numbers of 2.6−3.4 (Table S4), suggesting that the formation of Cr(III)-NOM-Fe colloids affected the coordination of $Cr_xFe_{1-x}(OH)_3$ particles. Inconsistent with the wet chemical results, the Fe(II) signal was not observed in XANES spectra. Possible explanations for this discrepancy may be related to the loss of aqueous Fe(II) during the collection of solid samples through centrifugation and the unintentional oxidation of Fe(II) during the sample transportation.

In summary, the smaller coordination numbers of Cr−Cr and Fe−Fe shells from EXAFS spectra indicate the close association of colloidal Cr(III) and colloidal Fe with NOM likely via carboxyl moieties, as previously reported.[85,86] This is also consistent with our recent work[26] showing the strong associations between Cr, Fe, and C at the nanoscale for Cr(III)-NOM-Fe colloids formed upon the reaction of Cr(VI) with NOM-Fe(II) colloids at anoxic−oxic interfaces, which was evidenced by ultrahigh-resolution aberration-corrected scanning transmission electron microscopy (Cs-STEM). Under oxic conditions, the colloids may be present as Cr(III)-NOM-Fe(III) ternary colloids or NOM-stabilized Cr(III)−Fe(III) colloids. Under anoxic conditions, the colloids may be a mixture of Cr(III)-NOM-Fe(II) colloids and NOM-stabilized Cr(III) or NOM-stabilized Fe(II) colloids. However, the EXAFS spectra did not allow us to differentiate these colloidal compositions within the resolution of the instrument. Further work is required to combine a suite of techniques [e.g., Cs-STEM, in situ XAFS, small-angle neutron scattering (SANS), and computational chemistry analysis] to decipher the molecular structure of Cr(III)-NOM-Fe colloids.

3.4. Environmental Implications. $Cr_xFe_{1-x}(OH)_3$, which is the most common reduction products of Cr(VI) by iron-bearing materials, has long been treated as the sink of Cr in subsurface environments. This work extended our knowledge of geochemical behavior of Cr by providing new information about the dissolution of $Cr_xFe_{1-x}(OH)_3$ precipitates and formation of Cr(III)-NOM-Fe colloids by NOM_{red} under anoxic conditions. NOM_{red} dissolves $Cr_xFe_{1-x}(OH)_3$ precipitates mainly via reductive dissolution, thus elevating the aqueous Cr(III) and Fe(III/II) concentrations. Complexation of Cr(III) and Fe(III/II) with NOM results in the formation of Cr(III)-NOM-Fe colloids that could enhance the mobility of Cr(III), thus increasing the potential risk of reoxidation of Cr(III) to Cr(VI) when accessing to strong oxidants (e.g., Mn-containing minerals).[20,43−45,87,88] Additionally, for the Cr(III) colloids formed under anoxic conditions, the concomitant Fe(II) allows for the formation of ROS when exposed to oxygen,[89−91] further giving rise to the potential reoxidation risk of Cr(III). Therefore, the formation and stability of Cr(III)-NOM-Fe colloids may control the final fate and transport of reduced Cr(III) in the management of subsurface Cr contaminated sites. We note that the high concentration of NOM used in this study may not occur in most natural

https://doi.org/10.1021/acsearthspacechem.2c00255
ACS Earth Space Chem. 2022, 6, 2995−3006

environments (e.g., 10−50 mg C/L in wetlands);[92] however, it is within the range of concentrations used in engineered Cr(VI)-remediation sites.[29,93] We realize that the natural subsurface environments are more complexed than the systems presented in this study, future work is needed to extend our framework by revealing the multiple factors such as NOM origins, pH, ionic strength and compositions, and more complicated redox-fluctuation conditions on the dissolution of $Cr_xFe_{1-x}(OH)_3$ precipitates and transport of Cr(III)-containing colloids.

4. CONCLUSIONS

This study, to the best of our knowledge, is the first to demonstrate the NOM-induced dissolution of $Cr_xFe_{1-x}(OH)_3$ precipitates and formation of Cr(III)-NOM-Fe colloids using different redox states of NOM under both oxic and anoxic conditions. Through a set of laboratory-scale batch experiments, we reveal that NOM dissolves $Cr_xFe_{1-x}(OH)_3$ precipitates via ligand-promoted dissolution under oxic conditions and via reductive dissolution under anoxic conditions. Under oxic conditions, NOM adsorbs at the surface of $Cr_xFe_{1-x}(OH)_3$ precipitates via complexation of functional groups with Cr and Fe atoms, leading to the dissolution of $Cr_xFe_{1-x}(OH)_3$ precipitates. However, under anoxic conditions, reduced NOM reduces structural Fe(III) of $Cr_xFe_{1-x}(OH)_3$, contributing to the reductive dissolution of $Cr_xFe_{1-x}(OH)_3$ and releasing Cr(III) and Fe(III/II) into the aqueous phase. Colloid chemistry analysis indicates that the aqueous Cr(III) and Fe(III/II) observed at higher NOM concentrations are in fact present as Cr(III)-NOM-Fe colloids, which constitute a large fraction of total Cr and Fe released from the $Cr_xFe_{1-x}(OH)_3$. Further characterization using cryogenic XPS and EXAFS collectively reveal that NOM closely associates with Cr and Fe atoms of Cr(III)-NOM-Fe colloids. Findings of this study provide insights into the dissolution of $Cr_xFe_{1-x}(OH)_3$ precipitates and properties of the resulting Cr(III)-containing colloids, which are critical for a more complete understanding of Cr cycling and improving Cr remediation strategies in redox-dynamic and organic-rich environments.

■ ASSOCIATED CONTENT

Supporting Information

The Supporting Information is available free of charge at https://pubs.acs.org/doi/10.1021/acsearthspacechem.2c00255.

Detailed method of XAFS analysis; characterization of synthesized $Cr_xFe_{1-x}(OH)_3$ precipitates; evolution of Fe(II) from $Cr_xFe_{1-x}(OH)_3$ precipitates with NOM; summary of the batch experiments for NOM-induced dissolution of $Cr_xFe_{1-x}(OH)_3$ precipitates; atom percentage of C, Cr, Fe, and O at different XPS probing depths; and parameters of the Cr and Fe K-edge XANES LCF and EXAFS modeling results (PDF)

■ AUTHOR INFORMATION

Corresponding Authors

Peng Liao − *State Key Laboratory of Environmental Geochemistry, Institute of Geochemistry, Chinese Academy of Sciences, Guiyang 550081, PR China;* orcid.org/0000-0001-6924-1097; Email: liaopeng@mail.gyig.ac.cn

Chongxuan Liu − *State Environmental Protection Key Laboratory of Integrated Surface Water-Groundwater Pollution Control, School of Environmental Science and Engineering, Southern University of Science and Technology, Shenzhen 518055, P. R. China;* orcid.org/0000-0002-7403-6001; Email: liucx@sustech.edu.cn

Authors

Binrui Li − *State Environmental Protection Key Laboratory of Integrated Surface Water-Groundwater Pollution Control, School of Environmental Science and Engineering, Southern University of Science and Technology, Shenzhen 518055, P. R. China*

Shaojian Zhang − *State Key Laboratory of Environmental Geochemistry, Institute of Geochemistry, Chinese Academy of Sciences, Guiyang 550081, PR China*

Peng Liu − *School of Environment, China University of Geosciences, Wuhan 430074, P. R. China;* orcid.org/0000-0002-2870-7193

Zhihang Ye − *School of Environment, China University of Geosciences, Wuhan 430074, P. R. China*

Complete contact information is available at: https://pubs.acs.org/10.1021/acsearthspacechem.2c00255

Author Contributions

‖B.L. and S.Z. contributed equally.

Notes

The authors declare no competing financial interest.

■ ACKNOWLEDGMENTS

This study was supported by the National Natural Science Foundation of China (nos. 42177237), the Program for Guangdong Introducing Innovative and Entrepreneurial Teams (2017ZT07Z479), the Science and Technology Planning Project of Guizhou Province (QianKeHeZhiCheng, 2022-217), and the Central Government Leading Local Science and Technology Development QianKeZhongYinDi (20214028). X-ray absorption spectroscopy analyses were performed at Beamlines 20BM of the Advanced Photon Source, Argonne National Laboratory.

■ REFERENCES

(1) Blowes, D. Tracking Hexavalent Cr in Groundwater. *Science* **2002**, *295*, 2024−2025.

(2) Ellis, A. S.; Johnson, T. M.; Bullen, D. T. Chromium Isotopes and the Fate of Hexavalent Chromium in the Environment. *Science* **2002**, *295*, 2060−2062.

(3) Wadhawan, A. R. S.; Stone, T.; Bouwer, E. J. Biogeochemical Controls on Hexavalent Chromium Formation in Estuarine Sediments. *Environ. Sci. Technol.* **2013**, *47*, 8220−8228.

(4) Palmer, C. D.; Wittbrodt, P. R. Processes Affecting the Remediation of Chromium-contaminated Sites. *Environ. Health Perspect.* **1991**, *92*, 25−40.

(5) Wielinga, B.; Mizuba, M. M.; Hansel, C. M.; Fendorf, S. Iron Promoted Reduction of Chromate by Dissimilatory Iron-reducing Bacteria. *Environ. Sci. Technol.* **2001**, *35*, 522−527.

(6) Barnhart, J. Chromium Chemistry and Implications for Environmental Fate and Toxicity. *J. Soil Contam.* **1997**, *6*, 561−568.

(7) Bond, D. L.; Fendorf, S. Kinetics and Structural Constraints of Chromate Reduction by Green Rusts. *Environ. Sci. Technol.* **2003**, *37*, 2750−2757.

(8) Legrand, L.; El Figuigui, A.; Mercier, F.; Chausse, A. Reduction of Aqueous Chromate by Fe(II)/Fe(III) Carbonate Green Rust:

Kinetic and Mechanistic Studies. *Environ. Sci. Technol.* **2004**, *38*, 4587−4595.
(9) Loyaux-Lawniczak, S.; Refait, P.; Ehrhardt, J.-J.; Lecomte, P.; Génin, J.-M. R. Trapping of Cr by Formation of Ferrihydrite during the Reduction of Chromate Ions by Fe(II)−Fe(III) Hydroxysalt Green Rusts. *Environ. Sci. Technol.* **2000**, *34*, 438−443.
(10) Skovbjerg, L. L.; Stipp, S. L. S.; Utsunomiya, S.; Ewing, R. C. The Mechanisms of Reduction of Hexavalent Chromium by Green Rust Sodium Sulphate: Formation of Cr-goethite. *Geochim. Cosmochim. Acta* **2006**, *70*, 3582−3592.
(11) Williams, A. G. B.; Scherer, M. M. Kinetics of Cr(VI) Reduction by Carbonate Green Rust. *Environ. Sci. Technol.* **2001**, *35*, 3488−3494.
(12) Ai, Z.; Cheng, Y.; Zhang, L.; Qiu, J. Efficient Removal of Cr(VI) from Aqueous Solution with Fe@Fe2O3 Core−Shell Nanowires. *Environ. Sci. Technol.* **2008**, *42*, 6955−6960.
(13) Singh, B.; Sherman, D. M.; Gilkes, R. J.; Wells, M. A.; Mosselmans, J. F. W. Incorporation of Cr, Mn and Ni into goethite (α-FeOOH): mechanism from extended X-ray absorption fine structure spectroscopy. *Clay Miner.* **2018**, *37*, 639−649.
(14) Trolard, F.; Bourrie, G.; Jeanroy, E.; Herbillon, A. J.; Martin, H. Trace Metals in Natural Iron Oxides from Laterites: A study Using Selective Kinetic Extraction. *Geochim. Cosmochim. Acta* **1995**, *59*, 1285−1297.
(15) Cornell, R. M.; Schwertmann, U.*The Iron Oxides: Structure, Properties, Reactions, Occurrences, and Uses*; Wiley-VCH, 2003.
(16) Eary, L. E.; Rai, D. Chromate Removal from Aqueous Wastes by Reduction with Ferrous Ion. *Environ. Sci. Technol.* **1988**, *22*, 972−977.
(17) Hu, Y.; Xue, Q.; Tang, J.; Fan, X.; Chen, H. New Insights on Cr(VI) Retention by Ferrihydrite in the Presence of Fe(II). *Chemosphere* **2019**, *222*, 511−516.
(18) Yu, G.; Fu, F.; Ye, C.; Tang, B. Behaviors and Fate of Adsorbed Cr(VI) during Fe(II)-induced Transformation of Ferrihydrite-humic Acid co-precipitates. *J. Hazard. Mater.* **2020**, *392*, 122272.
(19) Dai, C.; Zuo, X.; Cao, B.; Hu, Y. Homogeneous and Heterogeneous (Fex, Cr1-x)(OH)3 Precipitation: Implications for Cr Sequestration. *Environ. Sci. Technol.* **2016**, *50*, 1741−1749.
(20) Pan, C.; Liu, H.; Catalano, J. G.; Qian, A.; Wang, Z.; Giammar, D. E. Rates of Cr(VI) Generation from CrxFe1-x(OH)3 Solids upon Reaction with Manganese Oxide. *Environ. Sci. Technol.* **2017**, *51*, 12416−12423.
(21) Gustafsson, J. P.; Persson, I.; Oromieh, A. G.; van Schaik, J. W. J.; Sjöstedt, C.; Kleja, D. B. Chromium(III) Complexation to Natural Organic Matter: Mechanisms and Modeling. *Environ. Sci. Technol.* **2014**, *48*, 1753−1761.
(22) Kaczynski, S. E.; Kieber, R. J. Hydrophobic c18 Bound Organic Complexes of Chromium and Their Potential Impact on the Geochemistry of Cr in Natural Waters. *Environ. Sci. Technol.* **1994**, *28*, 799−804.
(23) Stewart, A. G.; Hudson-Edwards, K. A.; Dubbin, W. E. Effect of Desferrioxamine B and Suwannee River Fulvic Acid on Fe(III) Release and Cr(III) Desorption from Goethite. *Geochim. Cosmochim. Acta* **2016**, *178*, 62−75.
(24) Duckworth, O. W.; Akafia, M. M.; Andrews, M. Y.; Bargar, J. R. Siderophore-promoted Dissolution of Chromium from Hydroxide Minerals. *Environ. Sci.: Processes Impacts* **2014**, *16*, 1348−1359.
(25) Saad, E. M.; Sun, J.; Chen, S.; Borkiewicz, O. J.; Zhu, M.; Duckworth, O. W.; Tang, Y. Siderophore and Organic Acid Promoted Dissolution and Transformation of Cr(III)-Fe(III)-(oxy)hydroxides. *Environ. Sci. Technol.* **2017**, *51*, 3223−3232.
(26) Liao, P.; Pan, C.; Ding, W.; Li, W.; Yuan, S.; Fortner, J. D.; Giammar, D. E. Formation and Transport of Cr(III)-NOM-Fe Colloids upon Reaction of Cr(VI) with NOM-Fe(II) Colloids at Anoxic-Oxic Interfaces. *Environ. Sci. Technol.* **2020**, *54*, 4256−4266.
(27) Mackey, D. Trace Metals and the Productivity of Shelf Waters off North West Australia. *Mar. Freshw. Res.* **1984**, *35*, 505−516.
(28) Nakayama, E.; Kuwamoto, T.; Tsurubo, S.; Tokoro, H.; Fujinaga, T. Chemical speciation of chromium in sea water. *Anal. Chim. Acta* **1981**, *130*, 289−294.
(29) Buerge, I. J.; Hug, S. J. Influence of Organic Ligands on Chromium(VI) Reduction by Iron(II). *Environ. Sci. Technol.* **1998**, *32*, 2092−2099.
(30) Mattuck, R.; Nikolaidis, N. P. Chromium Mobility in Freshwater Wetlands. *J. Contam. Hydrol.* **1996**, *23*, 213−232.
(31) Icopini, G. A.; Long, D. T. Speciation of Aqueous Chromium by Use of Solid-Phase Extractions in the Field. *Environ. Sci. Technol.* **2002**, *36*, 2994−2999.
(32) Aeschbacher, M.; Sander, M.; Schwarzenbach, R. P. Novel Electrochemical Approach to Assess the Redox Properties of Humic Substances. *Environ. Sci. Technol.* **2010**, *44*, 87−93.
(33) Li, B.; Liao, P.; Xie, L.; Li, Q.; Pan, C.; Ning, Z.; Liu, C. Reduced NOM Triggered Rapid Cr(VI) Reduction and Formation of NOM-Cr(III) Colloids in Anoxic Environments. *Water Res.* **2020**, *181*, 115923.
(34) Jiang, J.; Kappler, A. Kinetics of Microbial and Chemical Reduction of Humic Substances: Implications for Electron Shuttling. *Environ. Sci. Technol.* **2008**, *42*, 3563−3569.
(35) Dunnivant, F. M.; Schwarzenbach, R. P.; Macalady, D. L. Reduction of Substituted Nitrobenzenes in Aqueous Solutions Containing Natural Organic Matter. *Environ. Sci. Technol.* **1992**, *26*, 2133−2141.
(36) Chen, J.; Gu, B.; Royer, R. A.; Burgos, W. D. The Roles of Natural Organic Matter in Chemical and Microbial Reduction of Ferric Iron. *Sci. Total Environ.* **2003**, *307*, 167−178.
(37) Lovley, D. R.Fe(III) and Mn(IV) Reduction. *Environmental Microbe-Metal Interactions*; Wiley, 2000; pp 1−30.
(38) Kappler, A.; Haderlein, S. B. Natural Organic Matter as Reductant for Chlorinated Aliphatic Pollutants. *Environ. Sci. Technol.* **2003**, *37*, 2714−2719.
(39) Aeschbacher, M.; Brunner, S. H.; Schwarzenbach, R. P.; Sander, M. Assessing the Effect of Humic Acid Redox State on Organic Pollutant Sorption by Combined Electrochemical Reduction and Sorption Experiments. *Environ. Sci. Technol.* **2012**, *46*, 3882−3890.
(40) Bauer, I.; Kappler, A. Rates and Extent of Reduction of Fe(III) Compounds and O2 by Humic Substances. *Environ. Sci. Technol.* **2009**, *43*, 4902−4908.
(41) Liao, P.; Li, W.; Wang, D.; Jiang, Y.; Pan, C.; Fortner, J. D.; Yuan, S. Effect of Reduced Humic Acid on the Transport of Ferrihydrite Nanoparticles under Anoxic Conditions. *Water Res.* **2017**, *109*, 347−357.
(42) Pan, C.; Troyer, L. D.; Liao, P.; Catalano, J. G.; Li, W.; Giammar, D. E. Effect of Humic Acid on the Removal of Chromium(VI) and the Production of Solids in Iron Electrocoagulation. *Environ. Sci. Technol.* **2017**, *51*, 6308−6318.
(43) Bartlett, R.; James, B. Behavior of Chromium in Soils: III. Oxidation. *J. Environ. Qual.* **1979**, *8*, 31−35.
(44) Liu, W.; Li, J.; Zheng, J.; Song, Y.; Shi, Z.; Lin, Z.; Chai, L. Different Pathways for Cr(III) Oxidation: Implications for Cr(VI) Reoccurrence in Reduced Chromite Ore Processing Residue. *Environ. Sci. Technol.* **2020**, *54*, 11971−11979.
(45) Landrot, G.; Ginder-Vogel, M.; Livi, K.; Fitts, J. P.; Sparks, D. L. Chromium(III) Oxidation by Three Poorly-Crystalline Manganese-(IV) Oxides. 1. Chromium(III)-Oxidizing Capacity. *Environ. Sci. Technol.* **2012**, *46*, 11594−11600.
(46) Saad, E. M.; Wang, X.; Planavsky, N. J.; Reinhard, C. T.; Tang, Y. Redox-Independent Chromium isotope Fractionation Induced by Ligand-promoted Dissolution. *Nat. Commun.* **2017**, *8*, 1590.
(47) Qian, A.; Pan, C.; Yuan, S.; Giammar, D. E. Cr(VI) Formation from CrxFe1-x(OH)3 Induced by Mn(II) Oxidation on the Surface of CrxFe1-x(OH)3. *ACS Earth Space Chem.* **2020**, *4*, 1558−1564.
(48) Papassiopi, N.; Vaxevanidou, K.; Christou, C.; Karagianni, E.; Antipas, G. S. E. Synthesis, Characterization and Stability of Cr(III) and Fe(III) hydroxides. *J. Hazard. Mater.* **2014**, *264*, 490−497.
(49) Hansel, C. M.; Wielinga, B. W.; Fendorf, S. Structural and Compositional Evolution of Cr/Fe Solids after Indirect Chromate

https://doi.org/10.1021/acsearthspacechem.2c00255
ACS Earth Space Chem. 2022, 6, 2995−3006

Reduction by Dissimilatory Iron-reducing Bacteria. *Geochim. Cosmochim. Acta* **2003**, *67*, 401−412.
(50) Liao, P.; Li, W.; Jiang, Y.; Wu, J.; Yuan, S.; Fortner, J. D.; Giammar, D. E. Formation, Aggregation, and Deposition Dynamics of NOM-Iron Colloids at Anoxic-Oxic Interfaces. *Environ. Sci. Technol.* **2017**, *51*, 12235−12245.
(51) Li, B.; Liao, P.; Liu, P.; Wang, D.; Ye, Z.; Wang, J.; Chen, J.; Ning, Z.; Jiang, Y.; Liu, C. Formation, aggregation, and transport of NOM-Cr(iii) colloids in aquatic environments. *Environ. Sci.: Nano* **2022**, *9*, 1133−1145.
(52) Liao, P.; Liang, Y.; Shi, Z. Impact of Divalent Cations on Dark Production of Hydroxyl Radicals from Oxygenation of Reduced Humic Acids at Anoxic-Oxic Interfaces. *ACS Earth Space Chem.* **2019**, *3*, 484−494.
(53) Wang, Z.; Tebo, B. M.; Giammar, D. E. Effects of Mn(II) on UO2 Dissolution under Anoxic and Oxic Conditions. *Environ. Sci. Technol.* **2014**, *48*, 5546−5554.
(54) Sharma, P.; Ofner, J.; Kappler, A. Formation of Binary and Ternary Colloids and Dissolved Complexes of Organic Matter, Fe and As. *Environ. Sci. Technol.* **2010**, *44*, 4479−4485.
(55) Tamura, H.; Goto, K.; Yotsuyanagi, T.; Nagayama, M. Spectrophotometric Determination of Iron(II) with 1,10-phenanthroline in the Presence of Large Amounts of Iron(III). *Talanta* **1974**, *21*, 314−318.
(56) Ye, Z.; Zhou, J.; Liao, P.; Finfrock, Y. Z.; Liu, Y.; Shu, C.; Liu, P. Metal (Fe, Cu, and As) Transformation and Association Within Secondary Minerals in Neutralized Acid Mine Drainage Characterized Using X-ray Absorption Spectroscopy. *Appl. Geochem.* **2022**, *139*, 105242.
(57) Zhou, Z.; Liu, P.; Wang, S.; Finfrock, Y. Z.; Ye, Z.; Feng, Y.; Li, X. Iron-modified Biochar-based Bilayer Permeable Reactive Barrier for Cr(VI) Removal. *J. Hazard. Mater.* **2022**, *439*, 129636.
(58) Sass, B. M.; Rai, D. Solubility of Amorphous Chromium(III)-iron(III) Hydroxide Solid Solutions. *Inorg. Chem.* **1987**, *26*, 2228.
(59) Tang, Y.; Michel, F. M.; Zhang, L.; Harrington, R.; Parise, J. B.; Reeder, R. J. Structural Properties of the Cr(III)−Fe(III) (Oxy)-hydroxide Compositional Series: Insights for a Nanomaterial "Solid Solution". *Chem. Mater.* **2010**, *22*, 3589−3598.
(60) Liao, P.; Yu, K.; Lu, Y.; Wang, P.; Liang, Y.; Shi, Z. Extensive Dark Production of Hydroxyl Radicals from Oxygenation of Polluted River Sediments. *Chem. Eng. J.* **2019**, *368*, 700−709.
(61) Yu, C.; Lu, Y.; Zhang, Y.; Qian, A.; Zhang, P.; Tong, M.; Yuan, S. Significant Contribution of Solid Organic Matter for Hydroxyl Radical Production during Oxygenation. *Environ. Sci. Technol.* **2022**, *56*, 11878−11887.
(62) Page, S. E.; Sander, M.; Arnold, W. A.; McNeill, K. Hydroxyl Radical Formation upon Oxidation of Reduced Humic Acids by Oxygen in the Dark. *Environ. Sci. Technol.* **2012**, *46*, 1590−1597.
(63) Ludwig, C.; Casey, W. H.; Rock, P. A. Prediction of Ligand-promoted Dissolution Rates from the Reactivities of Aqueous Complexes. *Nature* **1995**, *375*, 44−47.
(64) Wang, Z.; Schenkeveld, W. D. C.; Kraemer, S. M.; Giammar, D. E. Synergistic Effect of Reductive and Ligand-Promoted Dissolution of Goethite. *Environ. Sci. Technol.* **2015**, *49*, 7236−7244.
(65) Piepenbrock, A.; Schröder, C.; Kappler, A. Electron Transfer from Humic Substances to Biogenic and Abiogenic Fe(III) Oxyhydroxide Minerals. *Environ. Sci. Technol.* **2014**, *48*, 1656−1664.
(66) Papassiopi, N.; Gaitanarou, Z.; Xenidis, A. Stabilization of Chromium in the form of Mixed Fe(III)-Cr(III) Hydroxides. *Fresenius Environ. Bull.* **2012**, *21*, 2399.
(67) Frierdich, A. J.; Scherer, M. M.; Bachman, J. E.; Engelhard, M. H.; Rapponotti, B. W.; Catalano, J. G. Inhibition of Trace Element Release During Fe(II)-Activated Recrystallization of Al-, Cr-, and Sn-Substituted Goethite and Hematite. *Environ. Sci. Technol.* **2012**, *46*, 10031−10039.
(68) Hua, J.; Chen, M.; Liu, C.; Li, F.; Long, J.; Gao, T.; Wu, F.; Lei, J.; Gu, M. Cr Release from Cr-Substituted Goethite during Aqueous Fe(II)-Induced Recrystallization. *Minerals* **2018**, *8*, 367.
(69) Wolf, M.; Kappler, A.; Jiang, J.; Meckenstock, R. U. Effects of Humic Substances and Quinones at Low Concentrations on Ferrihydrite Reduction by Geobacter metallireducens. *Environ. Sci. Technol.* **2009**, *43*, 5679−5685.
(70) Daugherty, E. E.; Gilbert, B.; Nico, P. S.; Borch, T. Complexation and Redox Buffering of Iron(II) by Dissolved Organic Matter. *Environ. Sci. Technol.* **2017**, *51*, 11096−11104.
(71) Rose, A. L.; Waite, T. D. Kinetics of Iron Complexation by Dissolved Natural Organic Matter in Coastal Waters. *Mar. Chem.* **2003**, *84*, 85−103.
(72) Neil, C. W.; Ray, J. R.; Lee, B.; Jun, Y.-S. Fractal Aggregation and Disaggregation of Newly Formed Iron(III) (hydr)oxide Nanoparticles in the Presence of Natural Organic Matter and Arsenic. *Environ. Sci.: Nano* **2016**, *3*, 647−656.
(73) Karlsson, T.; Persson, P. Complexes With Aquatic Organic Matter Suppress Hydrolysis and Precipitation of Fe(III). *Chem. Geol.* **2012**, *322*−*323*, 19−27.
(74) Philippe, A.; Schaumann, G. E. Interactions of Dissolved Organic Matter with Natural and Engineered Inorganic Colloids: A Review. *Environ. Sci. Technol.* **2014**, *48*, 8946−8962.
(75) McNeill, L.; McLean, J.; Edwards, M.; Parks, J. State of the Science of Hexavalent Chromium in Drinking Water. *Water Res. Found.* **2012**, *6666*, 1−35.
(76) Bera, M. K.; Ninomiya, Y.; Higuchi, M. Constructing Alternated Heterobimetallic [Fe(II)/Os(II)] Supramolecular Polymers with Diverse Solubility for Facile Fabrication of Voltage-Tunable Multicolor Electrochromic Devices. *ACS Appl. Mater. Interfaces* **2020**, *12*, 14376−14385.
(77) Gerber, S. J.; Erasmus, E. Electronic Effects of Metal Hexacyanoferrates: An XPS and FTIR Study. *Mater. Chem. Phys.* **2018**, *203*, 73−81.
(78) Cui, X.; Hong, L.; Lin, X. Electrochemical Preparation, Characterization and Application of Electrodes Modified with Hybrid Hexacyanoferrates of Copper and Cobalt. *J. Electroanal. Chem.* **2002**, *526*, 115−124.
(79) Brown, G. E.; Calas, G.; Waychunas, G. A.; Petiau, J.Chapter 11. X-ray Absorption Spectroscopy and Its Application in Mineralogy and Geochemistr. In *Spectroscopic Methods in Mineralogy and Geology*; Frank, C. H., Ed.; De Gruyter, 2018; pp 431−512.
(80) Peterson, M. L.; Brown, G. E.; Parks, G. A. Direct XAFS evidence for heterogeneous redox reaction at the aqueous chromium/magnetite interface. *Colloids Surf., A* **1996**, *107*, 77−88.
(81) Downs, R. T.; Hall-Wallace, M. The American Mineralogist Crystal Structure database. *Am. Mineral.* **2003**, *88*, 247−250.
(82) Zhu, M.; Legg, B.; Zhang, H.; Gilbert, B.; Ren, Y.; Banfield, J. F.; Waychunas, G. A. Early Stage Formation of Iron Oxyhydroxides during Neutralization of Simulated Acid Mine Drainage Solutions. *Environ. Sci. Technol.* **2012**, *46*, 8140−8147.
(83) Mitsunobu, S.; Takahashi, Y.; Utsunomiya, S.; Marcus, M. A.; Terada, Y.; Iwamura, T.; Sakata, M. Identification and Characterization of Nanosized Tripuhyite in Soil near Sb Mine Tailings. *Am. Mineral.* **2011**, *96*, 1171−1181.
(84) Waychunas, G. A.; Kim, C. S.; Banfield, J. F. Nanoparticulate Iron Oxide Minerals in Soils and Sediments: Unique Properties and Contaminant Scavenging Mechanisms. *J. Nanoparticle Res.* **2005**, *7*, 409−433.
(85) Yang, J.; Xia, X.; Liu, J.; Wang, J.; Hu, Y. Molecular Mechanisms of Chromium(III) Immobilization by Organo-Ferrihydrite Co-precipitates: The Significant Roles of Ferrihydrite and Carboxyl. *Environ. Sci. Technol.* **2020**, *54*, 4820−4828.
(86) Xia, X.; Wang, J.; Hu, Y.; Liu, J.; Darma, A. I.; Jin, L.; Han, H.; He, C.; Yang, J. Molecular Insights into Roles of Dissolved Organic Matter in Cr(III) Immobilization by Coprecipitation with Fe(III) Probed by STXM-Ptychography and XANES Spectroscopy. *Environ. Sci. Technol.* **2022**, *56*, 2432−2442.
(87) Fandeur, D.; Juillot, F.; Morin, G.; Olivi, L.; Cognigni, A.; Webb, S. M.; Ambrosi, J.-P.; Fritsch, E.; Guyot, F.; Brown, J. G. E., Jr XANES Evidence for Oxidation of Cr(III) to Cr(VI) by Mn-Oxides

https://doi.org/10.1021/acsearthspacechem.2c00255
ACS Earth Space Chem. 2022, 6, 2995−3006

in a Lateritic Regolith Developed on Serpentinized Ultramafic Rocks of New Caledonia. *Environ. Sci. Technol.* **2009**, *43*, 7384−7390.
(88) Ivarsson, M.; Broman, C.; Holm, N. G. Chromite Oxidation by Manganese Oxides in Subseafloor Basalts and the Presence of Putative Fossilized Microorganisms. *Geochem. Trans.* **2011**, *12*, 5.
(89) Yu, C.; Zhang, Y.; Lu, Y.; Qian, A.; Zhang, P.; Cui, Y.; Yuan, S. Mechanistic Insight into Humic Acid-Enhanced Hydroxyl Radical Production from Fe(II)-Bearing Clay Mineral Oxygenation. *Environ. Sci. Technol.* **2021**, *55*, 13366−13375.
(90) Tong, M.; Yuan, S.; Ma, S.; Jin, M.; Liu, D.; Cheng, D.; Liu, X.; Gan, Y.; Wang, Y. Production of Abundant Hydroxyl Radicals from Oxygenation of Subsurface Sediments. *Environ. Sci. Technol.* **2016**, *50*, 214−221.
(91) Ma, S.; Tong, M.; Yuan, S.; Liu, H. Responses of the Microbial Community Structure in Fe(II)-Bearing Sediments to Oxygenation: The Role of Reactive Oxygen Species. *ACS Earth Space Chem.* **2019**, *3*, 738−747.
(92) Curtis, P. J.Climatic and Hydrologic Control of DOM Concentration and Quality in Lakes. In *Aquatic Humic Substances: Ecology and Biogeochemistry*; Hessen, D. O., Tranvik, L. J., Eds.; Springer Berlin Heidelberg: Berlin, Heidelberg, 1998; pp 93−105.
(93) Kunhikrishnan, A.; Choppala, G.; Seshadri, B.; Wijesekara, H.; Bolan, N. S.; Mbene, K.; Kim, W.-I. Impact of Wastewater Derived Dissolved Organic Carbon on Reduction, Mobility, and Bioavailability of As(V) and Cr(VI) in Contaminated Soils. *J. Environ. Manage.* **2017**, *186*, 183−191.
(94) Biesinger, M. C.; Brown, C.; Mycroft, J. R.; Davidson, R. D.; McIntyre, N. S. X-ray Photoelectron Spectroscopy Studies of Chromium Compounds. *Surf. Interface Anal.* **2004**, *36*, 1550−1563.
(95) Grosvenor, A. P.; Kobe, B. A.; Biesinger, M. C.; McIntyre, N. S. Investigation of Multiplet Splitting of Fe 2p XPS Spectra and Bonding in Iron Compounds. *Surf. Interface Anal.* **2004**, *36*, 1564−1574.
(96) Biesinger, M. C.; Payne, B. P.; Grosvenor, A. P.; Lau, L. W. M.; Gerson, A. R.; Smart, R. S. C. Resolving Surface Chemical States in XPS Analysis of First Row Transition Metals, Oxides and Hydroxides: Cr, Mn, Fe, Co and Ni. *Appl. Surf. Sci.* **2011**, *257*, 2717−2730.

https://doi.org/10.1021/acsearthspacechem.2c00255
ACS Earth Space Chem. 2022, 6, 2995−3006